



OPEN Comprehensive guidance for optimizing the colloidal quantum dot (CQD) Perovskite solar cells: experiment and simulation

Ali Memari¹, Mohammad Javadian Sarraf^{1✉}, Seyyed Javad Seyyed Mahdavi Chabok¹ & Leili Motevalizadeh²

CsPbI₃ perovskite quantum dots (CPQDs) have received great attention due to their potential in large-scale applications. Increasing the efficiency of CPQDs solar cells is an important issue that is addressed in this paper. Here, we have simulated a 14.61% colloidal CPQD solar cell with the least fitting parameter that shows the accuracy of the following results. The absorber layer properties are varied and different power conversion efficiency (PCE) is achieved for the new device. The results show that colloidal CsPbI₃ material properties have a significant effect on the PCE of the device. Finally, the optimized parameters for the absorber layer are listed and the optimum efficiency of 29.88% was achieved for this case. Our results are interesting that help the researchers to work on CsPbI₃ materials for the achievement of highly efficient, stable, large-scale, and flexible CPQDs solar cells.

Traditional energy generation from fossil fuels has a negative effect on the environment¹. Using renewable energy sources instead of fossil fuels is an important issue to overcome this problem in worldwide^{2,3}. Solar cells are the most important renewable source that can convert sunlight to electricity^{4–11}. Silicon solar cell technology is applicable for industrial applications due to long-term stability and high-power conversion efficiency (PCE)^{12,13}. High melting point temperature (1400 °C) and needing for expensive instruments for the fabrication of Si solar cells are the biggest challenge for the production of low-cost solar cells^{14,15}. Researchers are working on, low-temperature and easy fabrication of third-generation of solar cells. The most known and important of these types of solar cells are perovskites due to their suitable properties and efficiency achievement above 25% in a short time (nearly one decade)¹⁶. Recently perovskite quantum dots (PQDs) are received great attention¹⁷. Mainly *a*-CsPbI₃ material has been used as an absorber layer in PQDs due to its ideal bandgap of 1.73 eV^{18,19}. Suitable properties such as narrow photoluminescence (PL), high carrier mobility, tunable absorbance, and great defect tolerance enable low non-radiative recombination despite huge defect density¹⁸. Good crystallinity and morphological control are not necessary simultaneously for the film deposition of colloidal CsPbI₃ QDs and this feature makes them suitable for fabrication of large-scale devices via printing techniques¹⁸. Achievement to the efficiency of 16% for CsPbI₃ QD solar cells (more than PbS QDs) shows their high potential for next-generation QD solar cells²⁰. Hence the focus of this work is the work on simulation of CsPbI₃ QDs solar cells. Yuan et al.²¹ have fabricated CsPbI₃ perovskite quantum dot (QD) solar cells by using a series of dopant-free polymeric hole-transporting materials (HTMs) and they have improved charge extraction at QD/polymer interfaces and increased the efficiency to 13%. Mehrabian et al.²² have simulated perovskite quantum dot solar cells with three different absorber layers of CsPbI₃, FAPbI₃, and CsPbI₃/FAPbI₃, and they optimized their cell by defining the bilayer of the CsPbI₃/FAPbI₃ structure by optimization of band gap and they achieved the PCE of 18.55%. In this research, we have simulated the CsPbI₃ perovskite quantum dot, and compared it to experimental results, at the following, we have investigated the electro-optical properties of CsPbI₃ CQD on solar cell performance.

¹Department of Electrical Engineering, Mashhad Branch, Islamic Azad University, Mashhad, Iran. ²Department of Physics, Mashhad Branch, Islamic Azad University, Mashhad, Iran. ✉email: m.j.sarraf@mshdiau.ac.ir

Results and discussion

Numerical simulation and validation

SCAPS-1D (SCAPS 3306) was used for the simulations. This package solves the Poisson equation (Eq. (1)), and the continuity equation for holes and electrons (Eqs. (2) and (3)) by coupling with Shockley–Read–Hall (SRH) recombination statistics (related to defects in bulk and interfaces) (Eqs. (5) and (6))^{23–30}.

$$\frac{d^2}{dx^2} \Phi(x) = \frac{q}{\epsilon_0 \epsilon_r} (p(x) - n(x) + N_D - N_A + n_t^+ - n_t^-) \quad (1)$$

$$-\left(\frac{1}{q}\right) \frac{\partial J_p}{\partial x} - U_p + G = \frac{\partial p}{\partial t} \quad (2)$$

$$\left(\frac{1}{q}\right) \frac{\partial J_n}{\partial x} - U_n + G = \frac{\partial n}{\partial t} \quad (3)$$

$$U_n = U_p = R_{Bulk,SRH} + R_{Surface,SRH} \quad (4)$$

$$R_{Bulk,SRH} = \frac{np - n_i^2}{\tau_p(n + n_t) + \tau_n(p + p_t)} \quad (5)$$

$$R_{Surface,SRH} = \frac{np - n_i^2}{(n + n_{ts})/S_n + (p + p_t)/S_p} \quad (6)$$

In Eq. (1), parameter Φ is the electrostatic potential, q is the electrical charge, ϵ_r and ϵ_0 are the relative and the vacuum permittivity, p and n are hole and electron concentrations, N_D and N_A are charge impurities of donor and acceptor type, n_t^+ and n_t^- are hole and electron trap concentrations, respectively. In Eqs. (2) and (3); J_n and J_p are the electron and hole current densities. G is the generation rate. τ_n/τ_p , $R_{Surface}$, S_n/S_p , n_i , n_t/p_t , and n_{ts}/p_{ts} are the electron/hole lifetime, surface recombination rate, surface recombination velocity of the electrons/holes, the intrinsic carrier concentration, the bulk electron/hole concentration of the trap states, and surface trap state concentration, respectively. Figure 1a shows the structure of CsPbI₃ CQDs. The input data for the simulation is provided in Table 1, and simulation-experiment J-V comparison was shown in Fig. 1b.

The interfaces properties data are available in SI.

Experiment details

The SnO₂ nanoparticle solution was deposited on ITO with spin-coating method at 120 °C for 30 min. PCBM CB solution (5 mg/mL) was spin-coated with speed of 5000 rpm for 30 s. In the following, a dissolved solution of 1.2 M CsI, 0.6 M PbI₂, and 0.6 M PbBr₂ in DMSO was used for precursor solution, and then spin-coated at 1500 rpm and 4500 rpm for 15 s and 45 s, respectively. As an HTL layer, PTB₇ solution (10 mg/mL in chlorobenzene) was spin-coated on CSPbI₃ CQDs. Finally, MoO₃ (10 nm) and Ag (nm) electrodes were deposited via thermal evaporation³⁴.

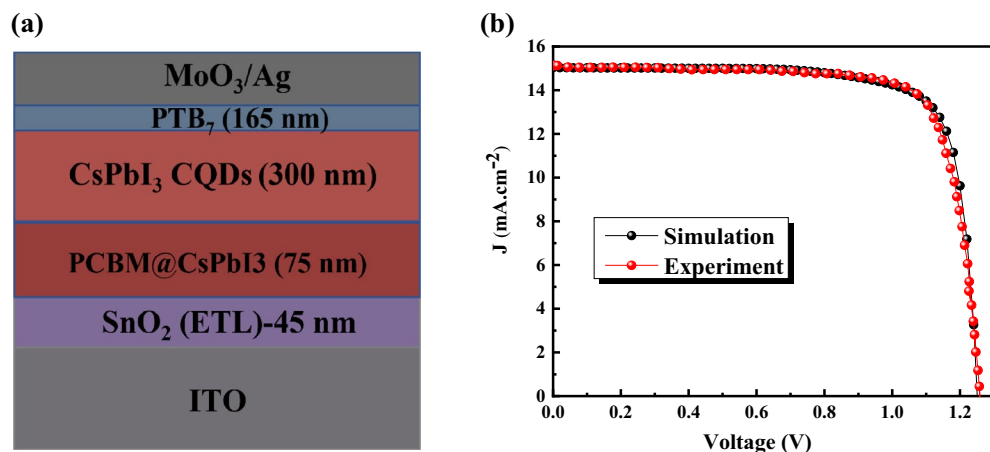


Figure 1. (a) Schematic of Perovskite quantum dot solar cells and (b) J-V characteristics of Perovskite quantum dot solar cells simulation and experiment.

Parameter and units	SnO ₂ (ETL)	PCBM@CsPbI ₃ (Buffer)	CsPbI ₃ CQDs (Absorber)	PtB ₇ (HTL)
Thickness (nm)	45 [experiment]	75 [experiment]	300 [experiment]	165 [experiment]
Electron affinity (eV)	4.5 [experiment]	4.25 [experiment]	3.99 [experiment]	3.45 [experiment]
Bandgap (eV)	3.6 [experiment]	2 [experiment]	1.76 [experiment]	1.63 [experiment]
Dielectric permittivity (relative)	9	4 ³¹	6 ³²	5 ³³
CB effective density of states (cm ⁻³)	2.2 × 10 ¹⁸ [Ref. ³²]	1.0 × 10 ²¹ ³¹	1.1 × 10 ²⁰ ³²	1.1 × 10 ²⁰ [fitting]
VB effective density of states (cm ⁻³)	1.8 × 10 ¹⁹ [Ref. ³²]	2 × 10 ²⁰ ³¹	8 × 10 ¹⁹ ³²	8 × 10 ¹⁹ [fitting]
Electron mobility (cm ² V ⁻¹ s ⁻¹)	100 [Ref. ³²]	1 × 10 ⁻²³ ¹	1.6 × 10 ¹³ ³²	1 × 10 ⁻²³ ³³
Hole mobility (cm ² V ⁻¹ s ⁻¹)	25 [Ref. ³²]	1 × 10 ⁻²³ ¹	1.6 × 10 ¹³ ³²	1 × 10 ⁻²³ ³³
Shallow uniform donor density N _D (cm ⁻³)	1.0 × 10 ²⁰ [Ref. ³²]	1.0 × 10 ²⁰ ³¹	0 ³²	0 ³³
Shallow uniform acceptor density N _A (cm ⁻³)	0 [Ref. ³²]	0 ³¹	1.0 × 10 ¹⁵ ³²	7.0 × 10 ¹⁶ ³³
Absorption constant A (cm ⁻¹ eV ^{-(1/3)})	file	1.0 × 10 ⁵	5.0 × 10 ⁵	1.0 × 10 ⁵
Absorption constant B (eV ^(1/3) .cm ⁻¹)	0	0	0	0
Electron thermal velocity (cm/s)	1.0 × 10 ⁷ [Ref. ³²]	1.0 × 10 ⁷	1.0 × 10 ⁷	1.0 × 10 ⁷
Hole thermal velocity (cm/s)	1.0 × 10 ⁷ [Ref. ³²]	1.0 × 10 ⁷	1.0 × 10 ⁷	1.0 × 10 ⁷
Electron Life Time (ns)	1.7 × 10 ⁻⁴ [fitting]	1 × 10 ⁻² [fitting]	2000 [fitting]	14 [fitting]
Hole Life Time (ns)	1.7 × 10 ⁻² [fitting]	1 × 10 ⁻² [fitting]	2000 [fitting]	14 [fitting]
Electron capture cross section (cm ²)	1.0 × 10 ⁻¹³ [fitting]	1.0 × 10 ⁻¹⁵ [fitting]	1.0 × 10 ⁻¹⁵ [fitting]	1.0 × 10 ⁻¹⁵ [fitting]
Hole capture cross section (cm ²)	1.0 × 10 ⁻¹⁵ [fitting]	1.0 × 10 ⁻¹⁵ [fitting]	1.0 × 10 ⁻¹⁵ [fitting]	1.0 × 10 ⁻¹⁵ [fitting]
Defect density (cm ⁻³)	6.0 × 10 ¹⁸ [fitting]	1.0 × 10 ¹⁹ [fitting]	5.0 × 10 ¹³ [fitting]	7.0 × 10 ¹⁵ [fitting]
Defect energy with respect to valence band energy E _v /type (eV)	+ 1.2(Single acceptor/Gauss)	+ 0.6/Neutral	+ 0.6/Neutral	+ 0.6/Neutral

Table 1. Input electro-optical parameters for the simulation. Data were extracted from valid references, experiment basic, and fittings.

Tuning properties of CsPbI₃ CQDs (absorber layer)

Effect of band gap

Here, we have studied the effect of band gap of CsPbI₃ CQDs. By increasing the band gap to value of 1.4 eV, the efficiency will increase to 21%. While, for band gap more than 1.4 eV, V_{oc} is increased to 1.2 V but the efficiency and J_{sc} is decreased and continued to reach 1%, and 3 mA/cm², respectively, for band gap of 2.5 eV (Fig. 2).

By varying the band gap, absorption coefficient also varied due to equation $(A + B/hv)\sqrt{(E_g - hv)}$. For understanding the behavior of band gap effect on performance, we plotted the band structure and electron Fermi level (Figs. 3 and 4) for two cases of high (E_g = 1.4 eV) and low efficiency (E_g = 2.5 eV). The valence band offset (VBO) between absorber and HTL is increased for the case of E_g = 1.5 eV that create a spike against hole transport (Fig. 3) and increase the recombination and leads to J_{sc}, FF, and efficiency decrement. The higher V_{oc} for the case of E_g = 1.5 eV, is due to electron fermi level increment.

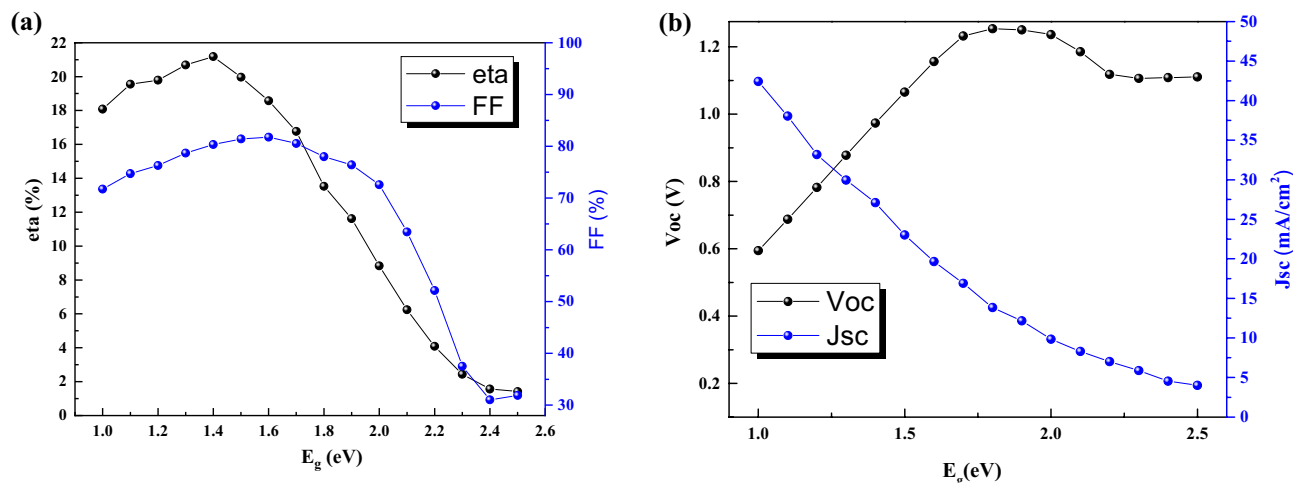


Figure 2. Effect of band gap of CsPbI₃ CQDs on J-V parameters.

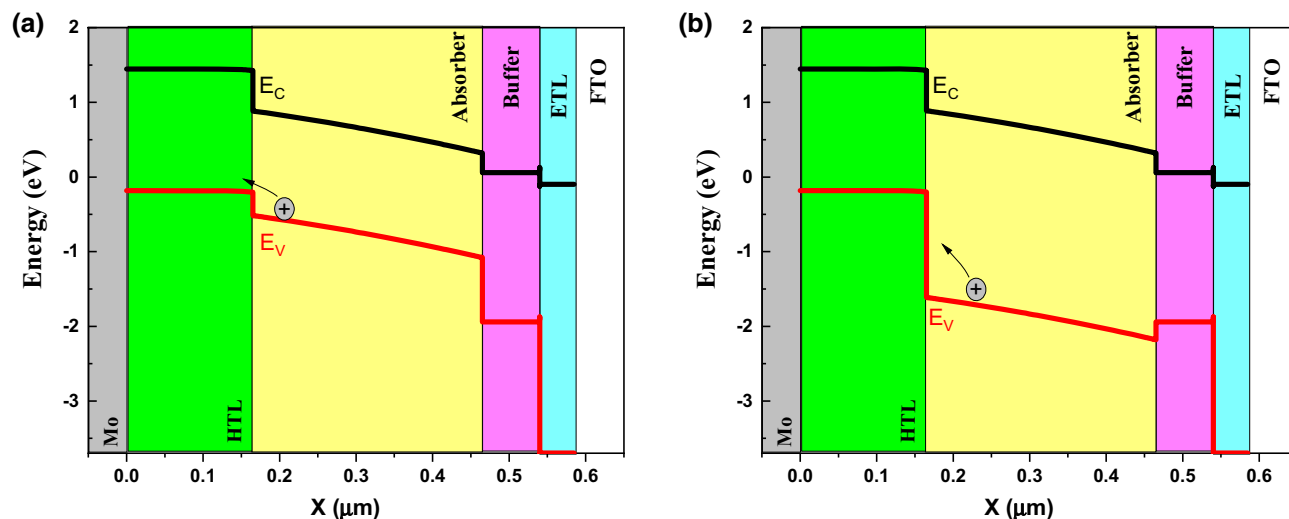


Figure 3. Band structure for band gap of (a) 1.4 eV, and (b) 2.5 eV. Graphs taken at $V=0$ V at light condition.

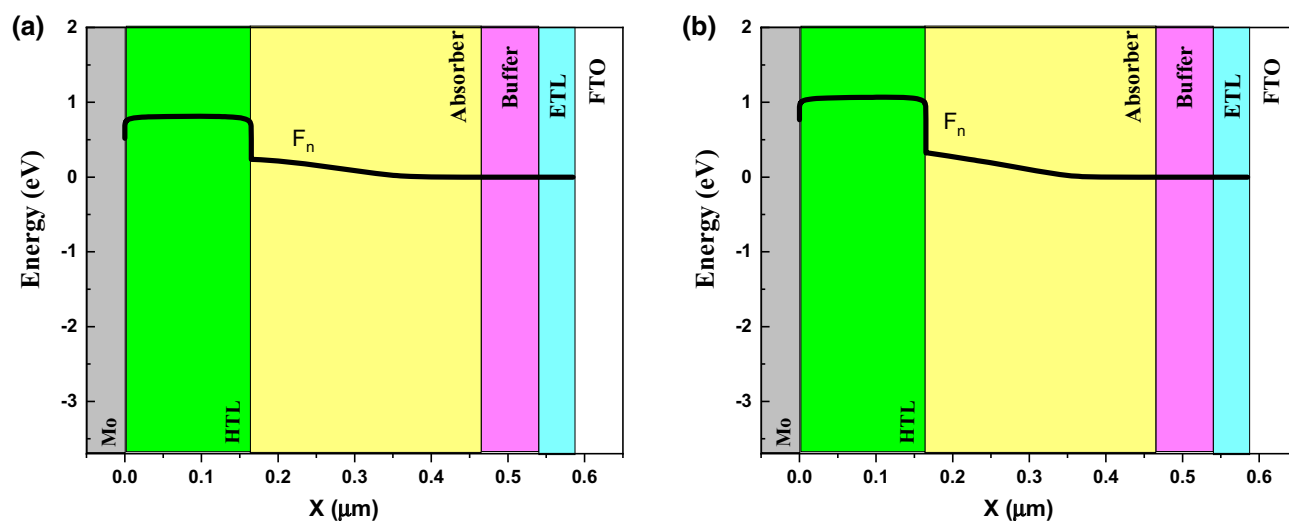


Figure 4. Electron Fermi level for band gap of (a) 1.4 eV, and (b) 2.5 eV. Graphs taken at $V=0$ V at light condition.

Effect of electron affinity

Here, we have modified the electron affinity of absorber layer from 2.7 to 4.5 eV (Fig. 5).

In electron affinity of 2.7 eV and 3.9 eV we have the lowest (0.81%) and highest efficiency (15.48%), respectively. By investigation of band structure, we found that the conduction band offset (CBO) between absorber and buffer in case of 3.9 eV, is in cliff form that help the electrons move easily and speedy (Fig. 6). For the case of 2.7 eV, the electrons in conduction band see a barrier and they are stuck which result in high recombination.

Effect of electron–hole mobility

Here, the effect of electron and hole mobility on performance are investigated. Electron mobility has low effect on performance (Fig. 7) and it because of the impurity of absorber layer that in p-type semiconductor hole mobility is important. Here, hole mobility has significant impact on J-V characteristics (Fig. 8). By increasing the hole mobility from $10^{-3} \text{ cm}^2\text{V}^{-1}\text{s}^{-1}$ to $10^3 \text{ cm}^2\text{V}^{-1}\text{s}^{-1}$ the efficiency is increased from 3.84% to 15.20%.

The recombination rate for the hole mobility of $10^{-3} \text{ cm}^2\text{V}^{-1}\text{s}^{-1}$ and $10^3 \text{ cm}^2\text{V}^{-1}\text{s}^{-1}$ is plotted in Fig. 9.

For low values of hole mobility, the recombination rate in perovskite layer is increased severely. Here, for fabrication of QD solar cells with high efficiency we need an absorber layer with high mobility.

Effect of acceptor density

We modified the doping of absorber layer, acceptor density, by increasing the density of absorber, efficiency, FF and V_{oc} are increased but J_{sc} decreases (Fig. 10).

As can be seen in Fig. 11, level of electron fermi is enhanced due to higher doping density that helps the electric field in the absorber layer and efficiency increment.

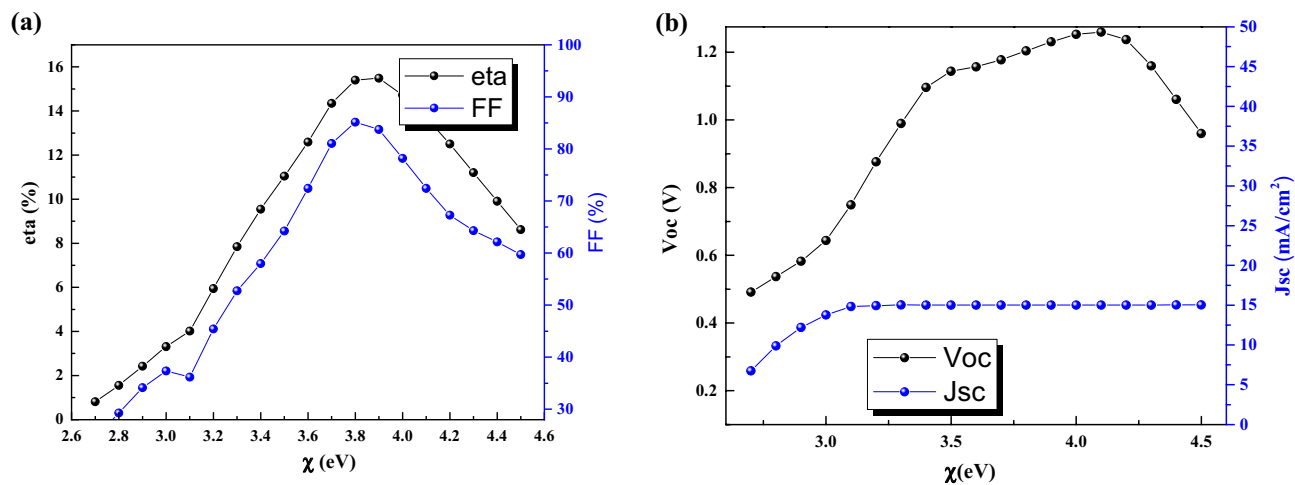


Figure 5. Effect of electron affinity of CsPbI₃ CQDs on J-V parameters.

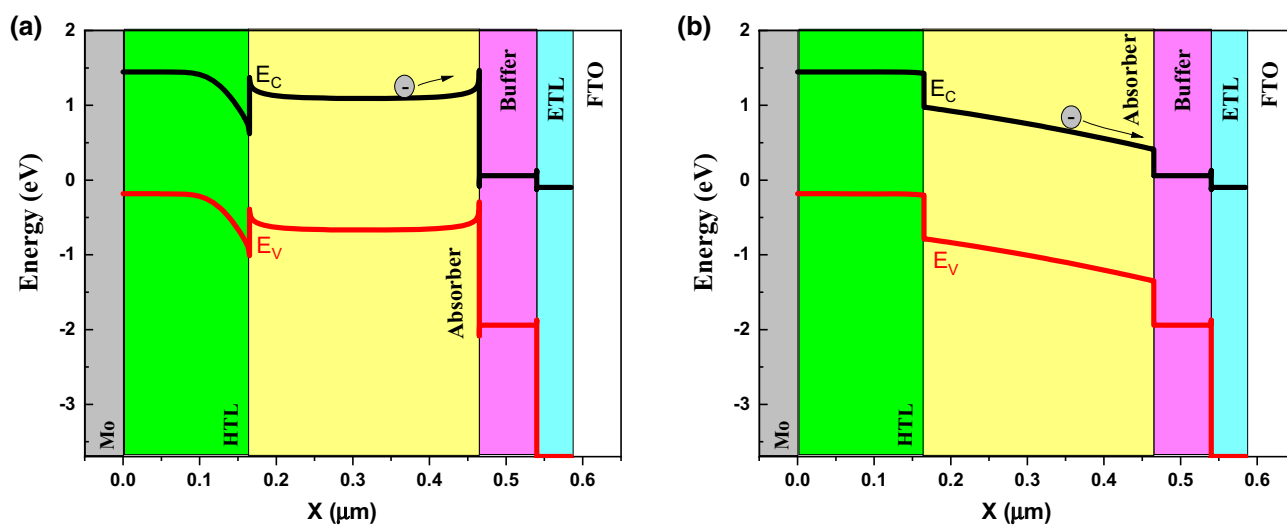


Figure 6. Band structure for electron affinity of (a) 2.7 eV, and (b) 3.9 eV. Graphs taken at $V = 0$ V at light condition.

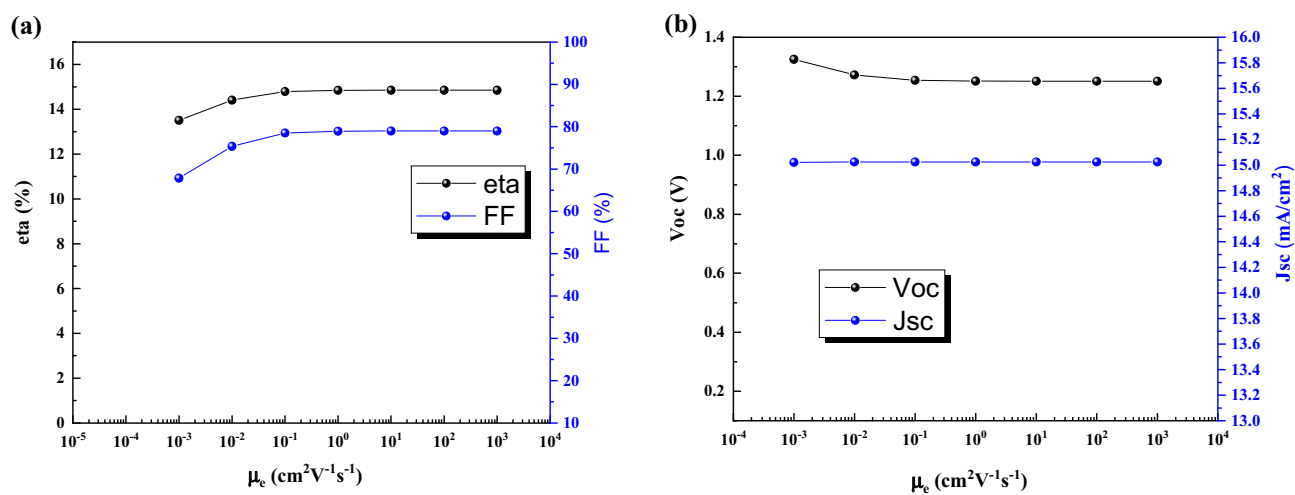


Figure 7. Effect of electron mobility of CsPbI₃ CQDs on J-V parameters.

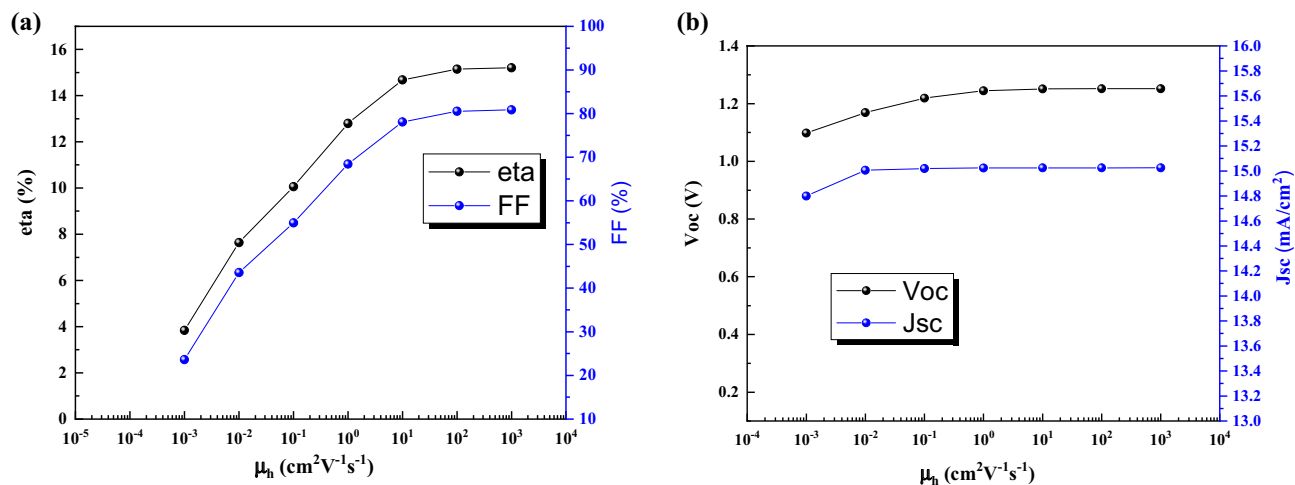


Figure 8. Effect of hole mobility of CsPbI₃ QCDs on J-V parameters.

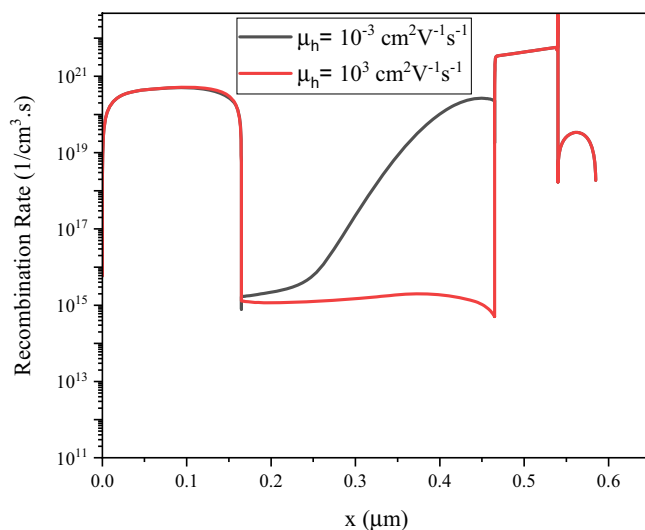


Figure 9. Recombination rate for the hole mobility of (a) 10^{-3} cm²V⁻¹s⁻¹ and (b) 10^3 cm²V⁻¹s⁻¹. Graphs taken at $V=0$ V at light condition.

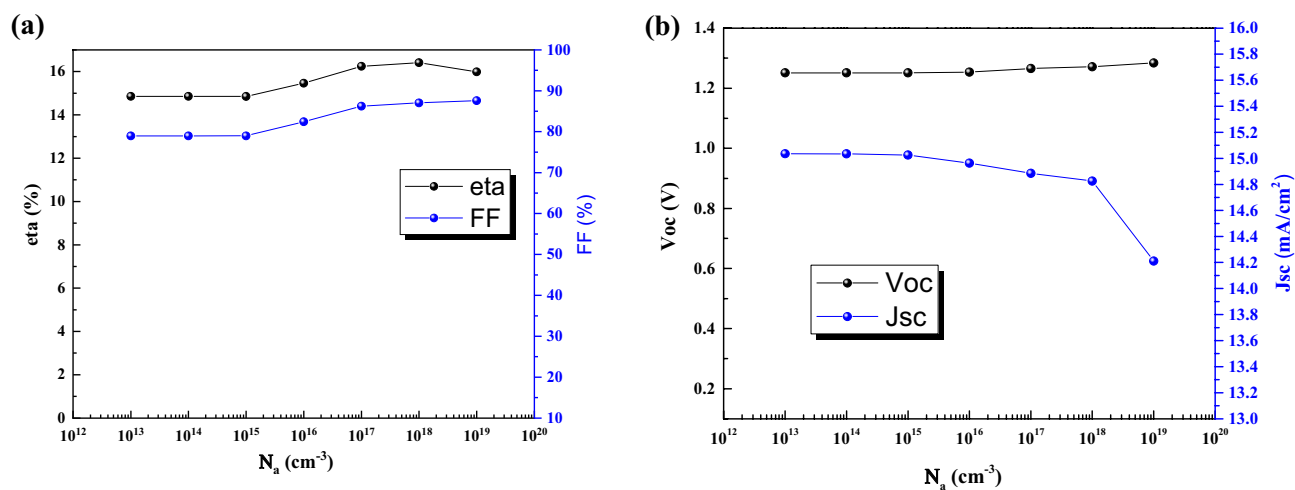


Figure 10. Effect of acceptor density of the absorber of CsPbI₃ QCDs on J-V parameters.

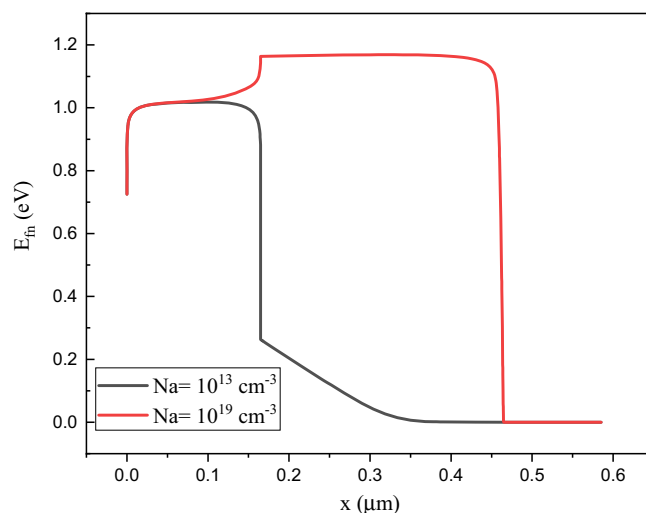


Figure 11. Electron Fermi level for $N_a =$ (a) 10^{13} cm^{-3} , and (b) 10^{19} cm^{-3} . Graphs taken at $V = 0 \text{ V}$ at light condition.

Effect of defect density

The defects formation are the most important factors to have high or low efficiency. Here, we have changed defects density from the low (10^{10} cm^{-3}) to high values (10^{20} cm^{-3}) (Fig. 12). The high population of defects are detrimental for the device that can reduce the efficiency from 0.12% to 16.49%. It means the high defect density can cause the solar cell device does not work efficiently.

The higher defect density will increase the recombination rate at perovskite layer (Fig. 13).

Effect of defect energy and types

Defect energy is important parameter which shows the types of defects in the QD perovskite layer. The defects with energy between 0.4 eV to 1.4 eV are harmful for device due to poor efficiency (Fig. 14).

This behavior is because of recombination rate enhancement.

For defect types we have consider 3 cases,

- I. $\sigma_n = \sigma_p$
 $\sigma_n = 10^{-15} \text{ cm}^2$, $\sigma_p = 10^{-15} \text{ cm}^2$, and $N_t = 10^{15} \text{ cm}^{-3}$ are considered for the below figures.
- II. $\sigma_n > \sigma_p$
 $\sigma_n = 10^{-14} \text{ cm}^2$, $\sigma_p = 10^{-15} \text{ cm}^2$, and $N_t = 10^{15} \text{ cm}^{-3}$ are considered for the below figures.
- III. $\sigma_n < \sigma_p$
 $\sigma_n = 10^{-15} \text{ cm}^2$, $\sigma_p = 10^{-14} \text{ cm}^2$, and $N_t = 10^{15} \text{ cm}^{-3}$ are considered for the below figures.

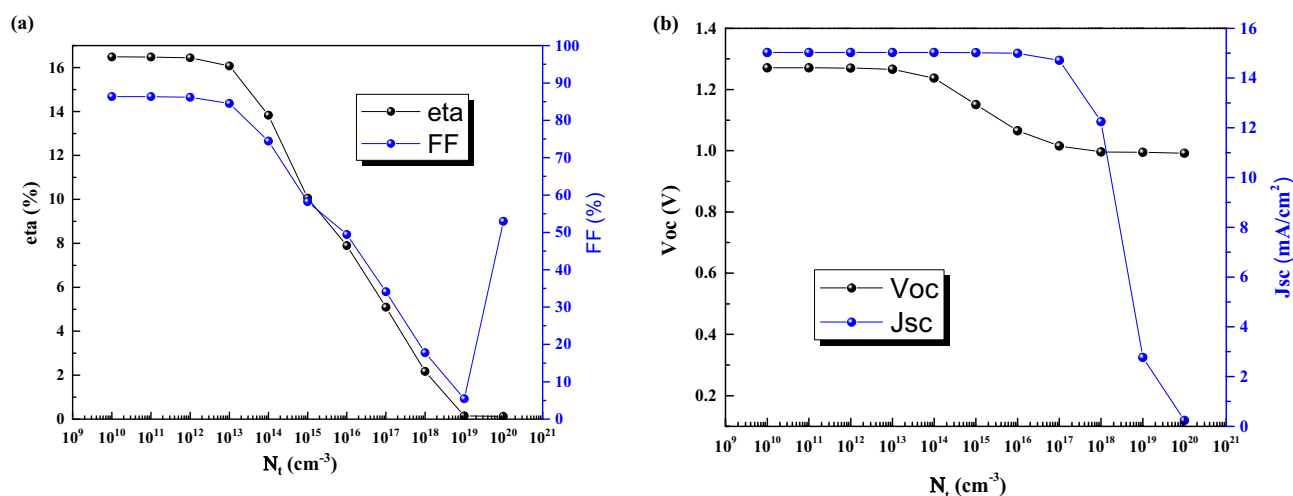


Figure 12. Effect of defect density of the absorber of CsPbI_3 CQDs on J–V parameters.

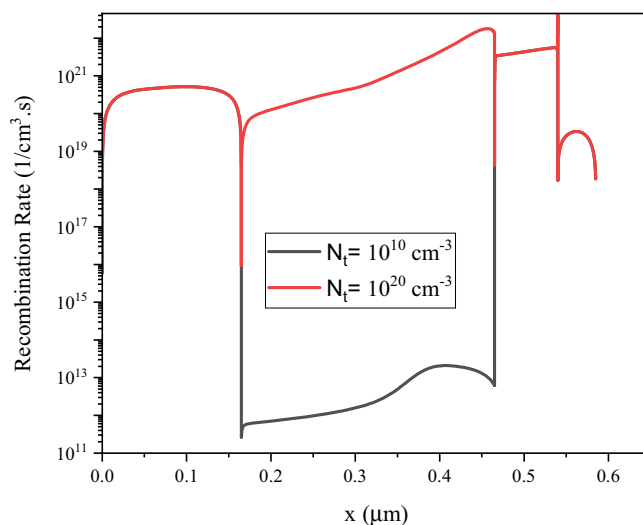


Figure 13. Recombination rate for the defect density of (a) 10^{10} cm^{-3} and (b) 10^{20} cm^{-3} . Graphs taken at $V = 0 \text{ V}$ at light condition.

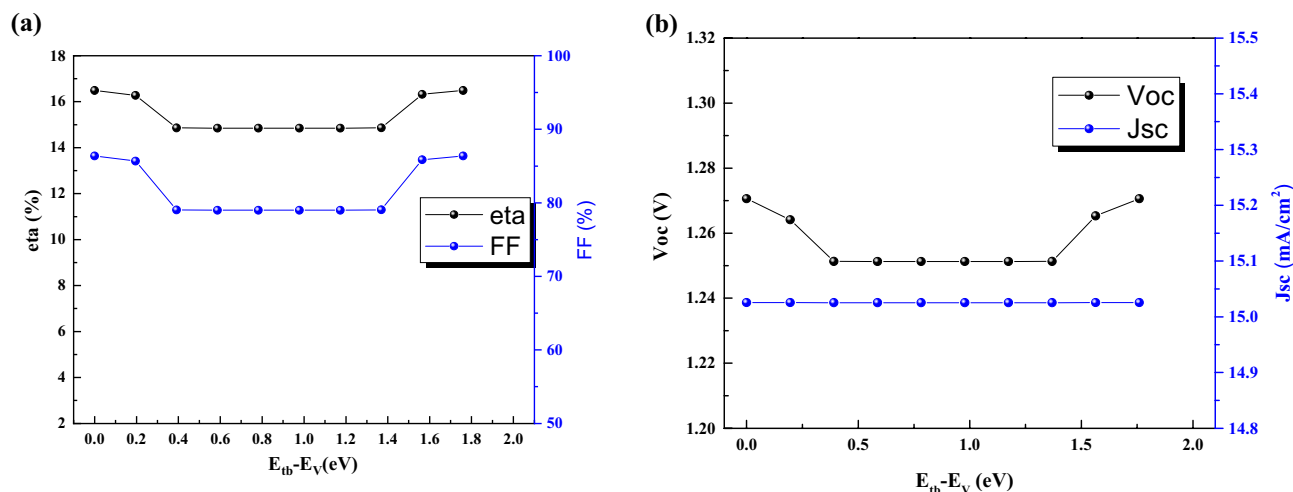


Figure 14. Effect of defect energy of the CsPbI_3 CQDs on J–V parameters.

As we see in 3 cases of I, II, and III (Figs. 15, 16, and 17), there is no significant effect on J–V parameters on 3 types of defects. However, in real situation it is important due to different density of defect (also we show this in previous section), but here we assume the same density for 3 cases of defect type.

Effect of thickness

The effect of thickness is investigated on J–V characteristics (Fig. 18). By increasing the thickness from 10 to 200 nm, the efficiency is enhanced drastically, and for the thickness higher than 200 nm, the efficiency will drop slowly. The thickness between 100 and 350 nm seems suitable for choosing CPQDs solar cells.

Optimized case

Finally, we optimized the cell by definition of new ETL, HTL and optimum electro-optical parameters for HTL/absorber, Buffer/absorber and absorber layer. The efficiency is enhanced from 14.85% to 29.88% (Fig. 19). This improvement eager the researcher to work on CQD Perovskite solar cell for industrial and marketing application in near future.

Conclusion

This study addressed the comprehensive investigation of absorber layer properties in CsPbI_3 perovskite quantum dots (CPQDs) solar cells. For the achievement of highly efficient CPQDs solar cells, it is important to choose absorber layer materials with a band gap of 1–1.7 eV, an electron affinity of 3.7–4 eV, and electron mobility (μ_e) of 10^{-2} – $10^3 \text{ cm}^2/\text{V.s}$, hole mobility (μ_h) of 10^1 – $10^3 \text{ cm}^2/\text{V.s}$, acceptor density (N_a) of 10^{13} – 10^{19} cm^{-3} , defect

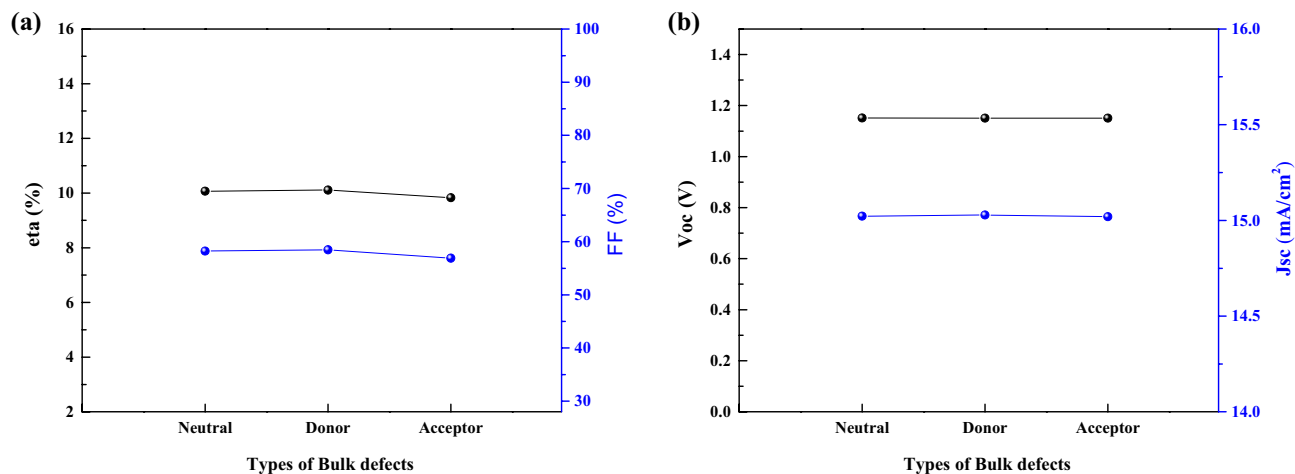


Figure 15. Effect of defect types of the CsPbI₃ CQDs on J–V parameters.

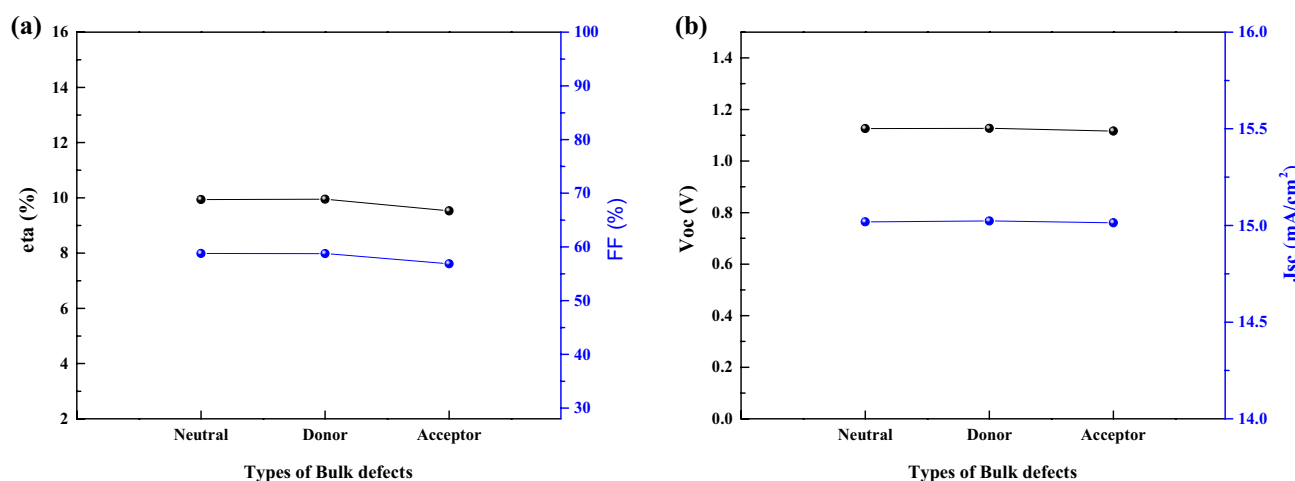


Figure 16. Effect of defect types of the CsPbI₃ CQDs on J–V parameters.

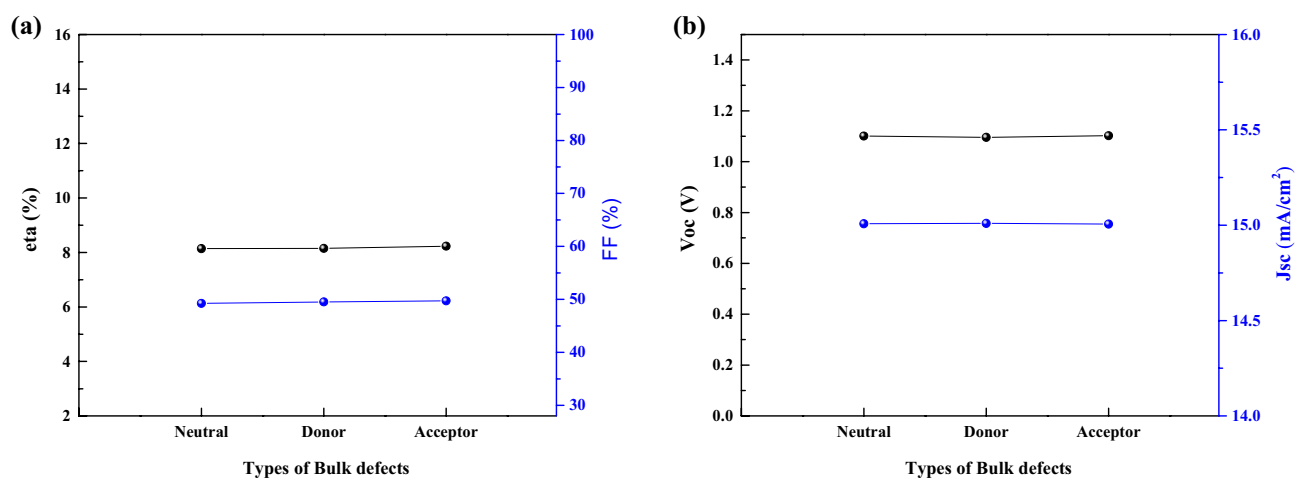


Figure 17. Effect of defect types of the CsPbI₃ CQDs on J–V parameters.

properties such as defect density of 10^{10} – 10^{13} cm⁻³, and Defect energy of 0–1.76 eV. For modifying the CsPbI₃ properties, the material ratio, deposition processes such as temperature and time of deposition, different treatments, adding nanoparticles such as graphene, and using stacked deposition with different sandwich materials are the ways that we have proposed for the modification. The optimum efficiency of 29.88% was achieved for the

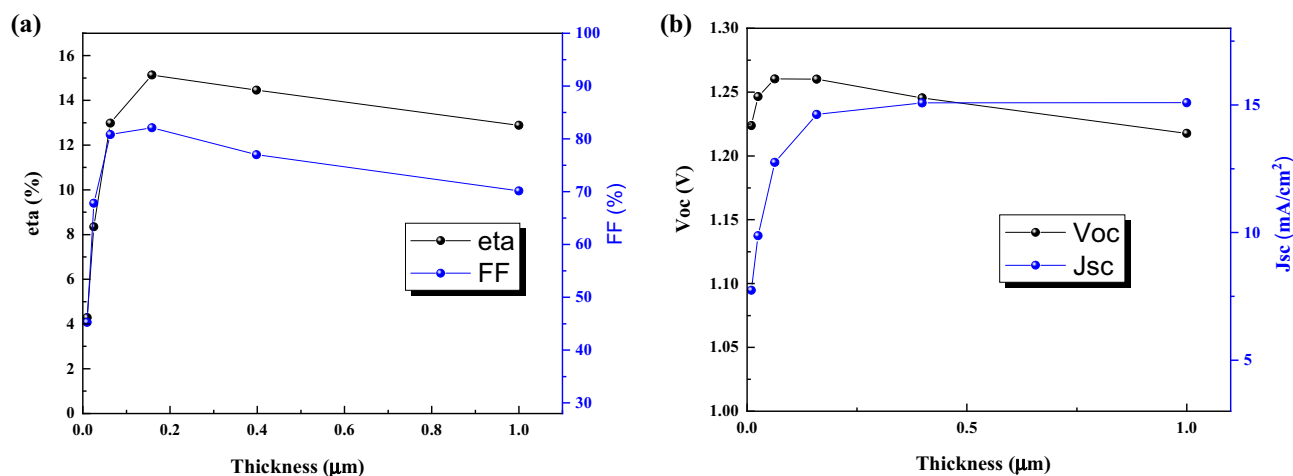


Figure 18. Effect of thickness of CsPbI₃ CQDs on J–V parameters.

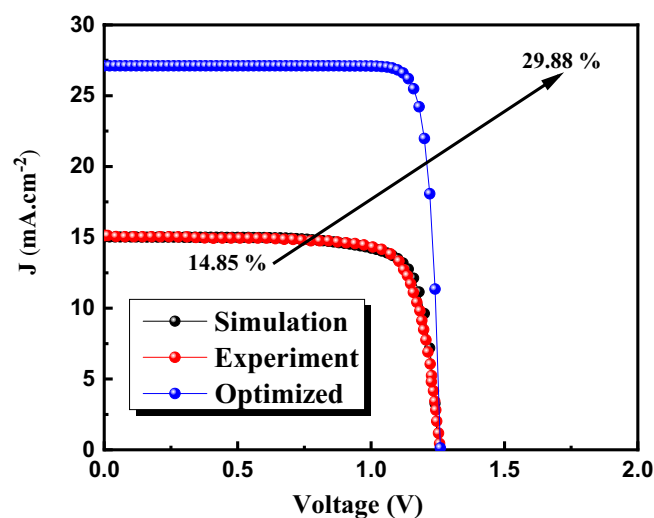


Figure 19. The J–V characteristics comparison between optimized, simulation and experiment case.

CPQD solar cell in this research. These results are very promising and eager the researcher work on our proposed model to achieve highly efficient CPQD solar cells.

Data availability

The data that support the findings of this study are available from the corresponding author, [M.J.S.], upon reasonable request.

Received: 12 June 2023; Accepted: 30 September 2023

Published online: 04 October 2023

References

- Voumik, L. C., Islam, M. A., Ray, S., Mohamed Yusop, N. Y. & Ridzuan, A. R. CO₂ emissions from renewable and non-renewable electricity generation sources in the G7 countries: Static and dynamic panel assessment. *Energies* **16**, 1044 (2023).
- Dresselhaus, M. S. & Thomas, I. L. Alternative energy technologies. *Nature* **414**, 332–337 (2001).
- Poizot, P. & Dolhem, F. Clean energy new deal for a sustainable world: from non-CO₂ generating energy sources to greener electrochemical storage devices. *Energy Environ. Sci.* **4**, 2003–2019 (2011).
- Hu, A. *et al.* Impact of solar panels on global climate. *Nat. Clim. Change* **6**, 290–294 (2016).
- Singh, G. K. Solar power generation by PV (photovoltaic) technology: A review. *Energy* **53**, 1–13 (2013).
- Wang, H., Yang, M., Cai, W. & Zang, Z. Suppressing phase segregation in CsPbI₃ Br₂ films via anchoring halide ions toward underwater solar cells. *Nano Lett.* **23**, 4479–4486 (2023).
- Chen, Z., Yang, M., Li, R., Zang, Z. & Wang, H. Double-side interface engineering synergistically boosts the efficiency of inorganic CsPbI₃ Br₂ perovskite solar cells over 12%. *Adv. Opt. Mater.* **10**, 2200802 (2022).
- Wang, H. *et al.* Interface modulator of ultrathin magnesium oxide for low-temperature-processed inorganic CsPbI₃ Br₂ perovskite solar cells with efficiency Over 11%. *Sol. RRL* **4**, 2000226 (2020).

9. Wang, H. *et al.* Challenges and strategies relating to device function layers and their integration toward high-performance inorganic perovskite solar cells. *Nanoscale* **12**, 14369–14404 (2020).
10. Minbashi, M. & Yazdani, E. Comprehensive study of anomalous hysteresis behavior in perovskite-based solar cells. *Sci. Rep.* **12**, 1–14 (2022).
11. Hashemi, M., Minbashi, M., Ghorashi, S. M. B. & Ghobadi, A. A modeling study on utilizing low temperature sprayed In₂S₃ as the buffer layer of CuBaSn (S, Se) solar cells. *Sci. Rep.* **11**, 1–11 (2021).
12. Saga, T. Advances in crystalline silicon solar cell technology for industrial mass production. *npg Asia Mater.* **2**, 96–102 (2010).
13. Del Canizo, C., Del Coso, G. & Sinke, W. C. Crystalline silicon solar module technology: Towards the 1€ per watt-peak goal. *Prog. Photovoltaics Res. Appl.* **17**, 199–209 (2009).
14. Beaucarne, G., Bourdais, S., Slaoui, A. & Poortmans, J. Thin-film polycrystalline Si solar cells on foreign substrates: Film formation at intermediate temperatures (700–1300°C). *Appl. Phys. A* **79**, 469–480 (2004).
15. Rath, J. K. Low temperature polycrystalline silicon: A review on deposition, physical properties and solar cell applications. *Sol. Energy Mater. Sol. Cells* **76**, 431–487 (2003).
16. Nrel Efficiency Chart. <https://www.nrel.gov/pv/cell-efficiency.html>. (2023).
17. Huang, H. *et al.* High-efficiency perovskite quantum dot photovoltaic with homogeneous structure and energy landscape. *Adv. Funct. Mater.* **33**, 2210728 (2023).
18. Khan, J., Ullah, I. & Yuan, J. CsPbI₃ perovskite quantum dot solar cells: Opportunities, progress and challenges. *Mater. Adv.* **3**, 1931–1952 (2022).
19. Memari, A., Sarraf, M. J., Chabok, S. J. S. M. & Motevalizadeh, L. Simulation and optimization of Perovskite-based CQDs solar cells. *Eur. Phys. J. Plus* **138**, 553 (2023).
20. Hao, M. *et al.* Ligand-assisted cation-exchange engineering for high-efficiency colloidal Cs_{1-x}FA_xPbI₃ quantum dot solar cells with reduced phase segregation. *Nat. Energy* **5**, 79–88 (2020).
21. Yuan, J. *et al.* Band-aligned polymeric hole transport materials for extremely low energy loss α -CsPbI₃ perovskite nanocrystal solar cells. *Joule* **2**, 2450–2463 (2018).
22. Mehrabian, M., Norouzi Afshar, E. & Norouzzadeh, P. Numerical simulation of bilayer perovskite quantum dot solar cell with 18.55% efficiency. *Opt. Quantum Electron* **54**, 439 (2022).
23. Burgelman, M., Verschraegen, J., Degreve, S. & Nollet, P. Modeling thin-film PV devices. *Prog. Photovoltaics Res. Appl.* **12**, 143–153 (2004).
24. Burgelman, M., Verschraegen, J., Minnaert, B. & Marlein, J. Numerical simulation of thin film solar cells: Practical exercises with SCAPS. *Proc. NUMOS. Univ. Gent* 357–366 (2007).
25. Kawano, Y., Chantana, J. & Minemoto, T. Impact of growth temperature on the properties of SnS film prepared by thermal evaporation and its photovoltaic performance. *Curr. Appl. Phys.* **15**, 897–901 (2015).
26. Ghobadi, A. *et al.* Simulating the effect of adding BSF layers on Cu₂BaSnS₃ thin film solar cells. *Opt. Mater. (Amst.)* **107**, 109927 (2020).
27. Fonash, S. J. 2010 Chapter Two - Material Properties and Device Physics Basic to Photovoltaics. in (ed. Fonash, S. J. B. T.-S. C. D. P. (Second E.)) (Academic Press, UK) 9–65. <https://doi.org/10.1016/B978-0-12-374774-7.00002-9>.
28. Burgelman, M. Mott-Schottky analysis from C-V simulations, and Admittance Analysis from C-f simulations in SCAPS. in 2–4 (Dept. of Electronics and Information Technology (ELIS), University of Gent, 'Belgium', 2017).
29. Park, Y. *et al.* Sputtered CdTe thin film solar cells with Cu₂Te/Au back contact. *Thin Solid Films* **546**, 337–341 (2013).
30. Sze, S. M. & Ng, K. K. *Physics of Semiconductor Devices* (Wiley, 2006).
31. Yue, M. *et al.* Optimizing the performance of CsPbI₃-based perovskite solar cells via doping a ZnO electron transport layer coupled with interface engineering. *Nano-Micro Lett.* **11**, 1–14 (2019).
32. Lin, L. *et al.* Simulated development and optimized performance of CsPbI₃ based all-inorganic perovskite solar cells. *Sol. Energy* **198**, 454–460 (2020).
33. Al Mubarak, M. *et al.* Molecular engineering in hole transport π -conjugated polymers to enable high efficiency colloidal quantum dot solar cells. *Adv. Energy Mater.* **10**, 1902933 (2020).
34. Hu, L. *et al.* Flexible and efficient perovskite quantum dot solar cells via hybrid interfacial architecture. *Nat. Commun.* **12**, 466 (2021).

Author contributions

A.M. and M.J.S. wrote the main manuscript text. A.M. provided the simulation results and prepared all the figures. M.J.S. provided guidance and supervision. S.J.S.M.C. and L.M. provided review and editing. All the authors reviewed the manuscript.

Competing interests

The authors declare no competing interests.

Additional information

Correspondence and requests for materials should be addressed to M.J.S.

Reprints and permissions information is available at www.nature.com/reprints.

Publisher's note Springer Nature remains neutral with regard to jurisdictional claims in published maps and institutional affiliations.



Open Access This article is licensed under a Creative Commons Attribution 4.0 International License, which permits use, sharing, adaptation, distribution and reproduction in any medium or format, as long as you give appropriate credit to the original author(s) and the source, provide a link to the Creative Commons licence, and indicate if changes were made. The images or other third party material in this article are included in the article's Creative Commons licence, unless indicated otherwise in a credit line to the material. If material is not included in the article's Creative Commons licence and your intended use is not permitted by statutory regulation or exceeds the permitted use, you will need to obtain permission directly from the copyright holder. To view a copy of this licence, visit <http://creativecommons.org/licenses/by/4.0/>.

© The Author(s) 2023